Assessment of Multiaxial Mechanical Response of Rigid Polyurethane Foams

Valeria Pettarin, Laura A. Fasce & Patricia M. Frontini

Journal of Materials Engineering and Performance

ISSN 1059-9495
Volume 23
Number 2

J. of Materi Eng and Perform (2014)
23:477-485
DOI 10.1007/s11665-013-0542-y

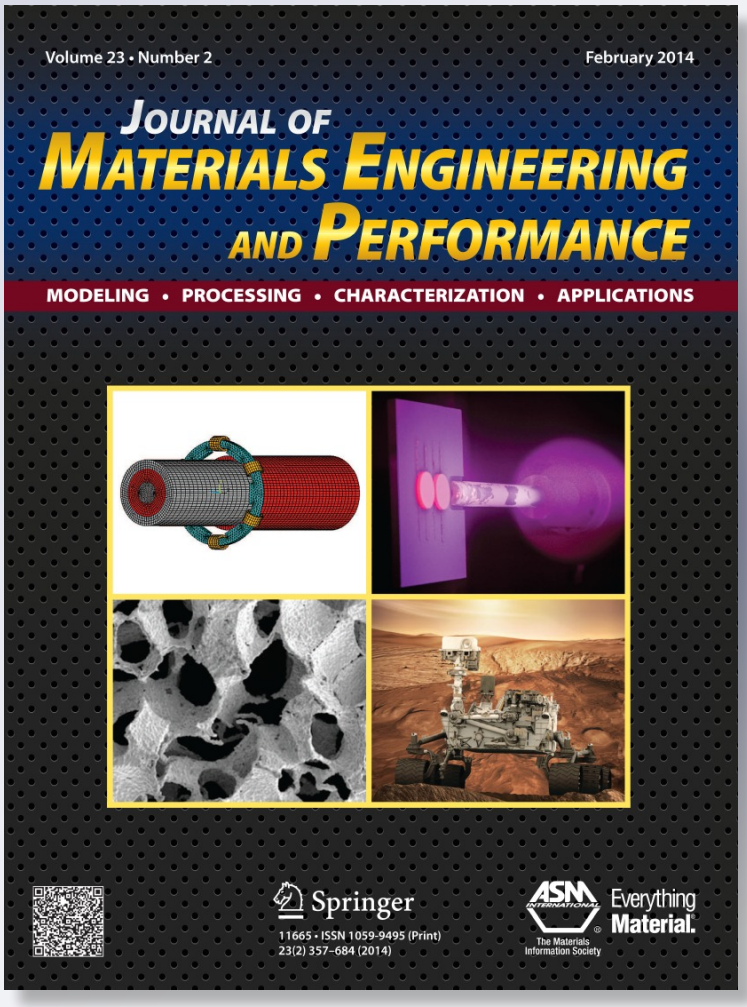

Springer

JMEPEG (2014) 23:477–485
DOI: 10.1007/s11665-013-0542-y

1059-9495/$19.00

Assessment of Multiaxial Mechanical Response of Rigid Polyurethane Foams

Valeria Pettarin, Laura A. Fasce, and Patricia M. Frontini

(Submitted December 18, 2012; in revised form February 18, 2013; published online April 12, 2013)

Multiaxial deformation behavior and failure surface of rigid polyurethane foams were determined using standard experimental facilities. Two commercial foams of different densities were assayed under uniaxial, biaxial, and triaxial stress states. These different stress states were reached in a uniaxial universal testing machine using suitable testing configurations which imply the use of special grips and lateral restricted samples. Actual strains were monitored with a video extensometer. Polyurethane foams exhibited typical isotropic brittle behavior, except under compressive loads where the response turned out to be ductile. A general failure surface in the stress space which accounts for density effects could be successfully generated. All of failure data, determined at the loss of linear elasticity point, collapsed in a single locus defined as the combination of a brittle crushing of closed-cell cellular materials criterion capped by an elastic buckling criterion.

Keywords failure, foam testing, mechanical properties, polyurethane

1. Introduction

Rigid polymer foams are currently being used as core materials in sandwich structures for aerospace, marine, automobiles, and petroleum industry (Ref 1-3). In many of these engineering applications foams are subjected to multiaxial stresses (Ref 4). Consequently, a proper design would require the knowledge of the multiaxial mechanical response of these materials.

The analysis of the physical mechanisms responsible for the homogeneous deformation of three-dimensional rigid closed-cell and flexible open-cell foams has already been well established, relating a well-defined mechanism with each mode of deformation. The elastic modulus of these materials, which are assumed as general orthotropic bodies, are related to the bending stiffness of the members composing the cell walls, whereas the elastic collapse of these materials is caused by elastic buckling of these members and the plastic collapse is introduced by plastic hinges formed inside these members. Experimental results in the literature show that depending on the nature of the solids from which they are made and on their relative density, foams could fail by several mechanisms, namely, elastic buckling, plastic yielding, brittle crushing or brittle fracture (Ref 5). Despite different models have been suggested, related to the statistical distribution of the directions of the cell struts in any cross section area (Ref 6), generally the foam structure is idealized by cubic arrays of members with adjoining cells arranged at a staggered position so that members meet each other at midpoints.

Failure mechanisms depend on the state of stress applied to the foam, it may be plastic in compression but brittle in tension. A compressive loading creates different regimes of mechanical behavior of cell and foam materials. Initially linear elasticity is dominated primarily by cell wall bending, whereas plastic deformation is associated with progressive crushing of cells. Sharp stresses increase for rather small deformations at the end of the loading history of the material results from the densification of the cell structure. On the other hand, tensile loading develops an initial linear elastic regime caused by cell wall bending which ends by a fast brittle fracture due to rapid and catastrophic development of microscopic cracks. Even when some foams may present only small differences in strengths under tension and compression, in every case these differences are sufficient to create the so-called strength differential effect.

Hence, it is the stresses combination causing failure which is important to the designer. This combination, when plotted in stress space, defines the so-called failure surface or envelope. When talking about cellular solids, it is given by the inner envelope of failure surfaces corresponding to each individual failure mechanism.

The mechanical properties and structural response of foams depend also on foam density, cell structure (such as cell size and shape, open or closed-cell, cells' orientation) (Ref 7), and solid material. Due to the viscoelastic nature of solid polymers, polymer foams often exhibit strain-rate dependent behavior, as well. When using closed-cell polymers foams, the presence of occluded gases within the cells may also have an influence itself.

Many efforts were devoted in the past to understand the behavior of cellular materials (Ref 8-17) like polymeric and metallic foams or wood. They derived in several theoretical and phenomenological models (Ref 5, 14, 15, 18-20) useful at the time of proposing any particular failure criteria.

Valeria Pettarin, Laura A. Fasce, and **Patricia M. Frontini**, Polymer Science and Engineering Group, INTEMA (University of Mar del Plata and National Research Council), Av. Juan B. Justo 4302, B7608FDQ Mar del Plata, Argentina. Contact e-mails: pettarin@fi.mdp.edu.ar, lfasce@fi.mdp.edu.ar, and pmfronti@fi.mdp.edu.ar.

The stress tensor $\underline{\sigma}$ and strain tensor $\underline{\varepsilon}$, of numerical models $\underline{\sigma} = f(\underline{\varepsilon})$ are linked by the so-called material constants or mechanical parameters. The assessment of the deformation behavior and failure surface of a cellular material requires to determine $\underline{\sigma}'$- $\underline{\varepsilon}$ plots and failure stresses under different stress states. In addition, mechanical parameters must be identified as functions of variables such as the strain rate, temperature, and density of the cellular material as well.

This implies the need of performing a number of rather complex mechanical tests in order to determine the model parameters. To carry out mechanical testing of polymer foams may be a difficult task (Ref 21) especially when multiaxial loading is needed. Even if standard mechanical tests like tensile test may appear simple to perform for other materials, gripping foams to apply tensile loading is complex due to foam inherent brittleness. If true stress is intended to be determined, knowledge of the lateral strains is also required but the attachment of mechanical extensometers has the drawbacks that it may influence the load-displacement curve and rupture point. Furthermore, measurements of multiaxial responses require multiaxial testing machines or special mechanical devices that may be expensive or difficult to make (Ref 13, 22-24).

Due to the inherent difficultness of performing tests under multiaxial stress states, i.e., measurements of loads and strains in more than one direction, some authors turn to the inverse approach to determine the model parameters (Ref 25). However, the development of a framework for robust and unbiased assessment of curve analysis performance it could be critical especially for methods involving the simultaneous determination of several parameters.

The purpose of this work is to determine the multiaxial deformation behavior of rigid polymeric foams by using standard experimental facilities. To this aim two commercial rigid polyurethane foams differing in foam density were assayed under uniaxial, biaxial, and triaxial stress states. Finally, a general failure surface in the stress space which accounts for density effects was constructed by using multiaxial failure data.

2. Experimental

2.1 Materials

Experiments were performed on two commercial fully cross-linked rigid PUR closed-cell foams differing in density: PUR-150 (ρ = 150 kg/m^3 and relative density ρ/ρ_s = 0.125, being the density of solid PUR ρ_s = 1200 kg/m^3 (Ref 23)) and PUR-75 (ρ = 75 kg/m^3 and ρ/ρ_s = 0.0625). Scanning electron microscopy (SEM) examination showed almost circular closed-cell structure with a cell diameter close to 500 μm and a wall thickness less than 1 μm (Fig. 1).

2.2 Mechanical Testing

Specimens for mechanical tests were cut off from 40 cm × 40 cm × 10 cm plaques along foam growing direction (GD) and the transversal direction (TD).

All mechanical tests were carried out at room temperature at 1 and 5 mm/min in an Instron 4467 universal testing machine. At least five samples were tested in each configuration. Strains were measured by means of a home-made video extensometer (Ref 26). Four ink dots of 1 mm diameter printed on the samples prior to deformation were monitored by a video camera interfaced with a fast image processor (resolution 720 × 480 pixels) which analyses in real time the distance in pixels, λ_i, between the center of gravity of two particular dots aligned along the stretching or transverse direction, giving engineering strains as

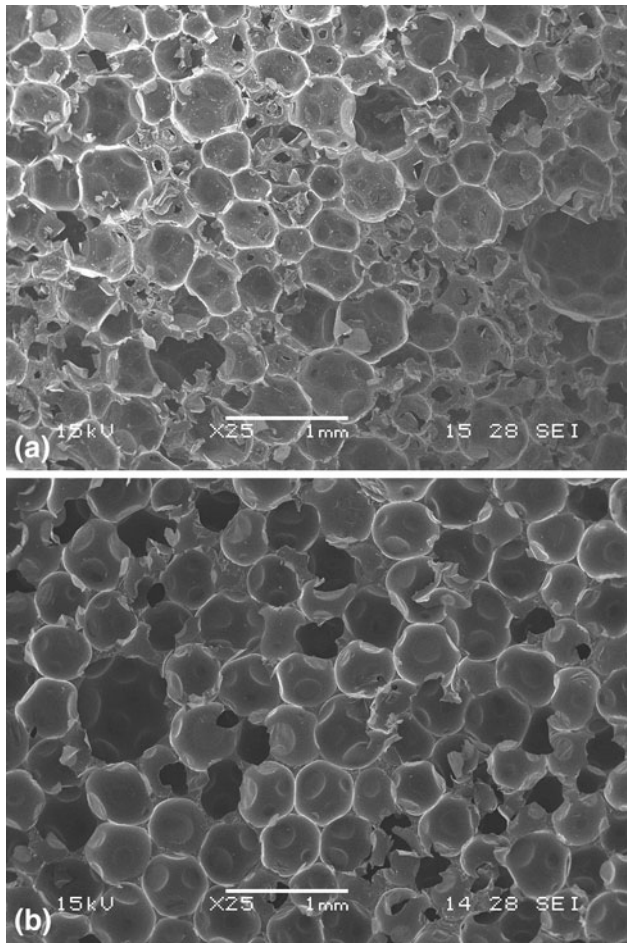

Fig. 1 SEM micrographs showing cell structure of (a) PUR-75 (b) PUR-150

$$\varepsilon_i = \frac{\Delta\lambda_i}{\lambda_{i0}} \qquad \text{(Eq 1)}$$

Given the distance between the center of gravity of dots (approximately 200 pixels) and the sensitivity of movement (1 pixel), the accuracy of strain measurements is about 5×10^{-3}.

After testing, deformed samples were examined by SEM on a JEOL JMS-5300 instrument with a voltage of 15 kV, after coating them with a thin gold layer.

2.2.1 Uniaxial Tests. Prismatic strips were used to prepare *uniaxial tension* specimens (Fig. 2a). Strips were tabbed with 50 mm long glass/epoxy tabs which were bonded over a length of 20 mm at the specimen ends with epoxy adhesive (Dicast RA1241/Dicure 354). The space between the extended parts of the tabs was filled in with high modulus epoxy filler (Dipoxit 205/Dicure 353). Specimens were gripped over the extended and filled portion of the tabs to avoid crushing of the foam. The values of the Poisson's ratio ν were obtained from these uniaxial tensile tests.

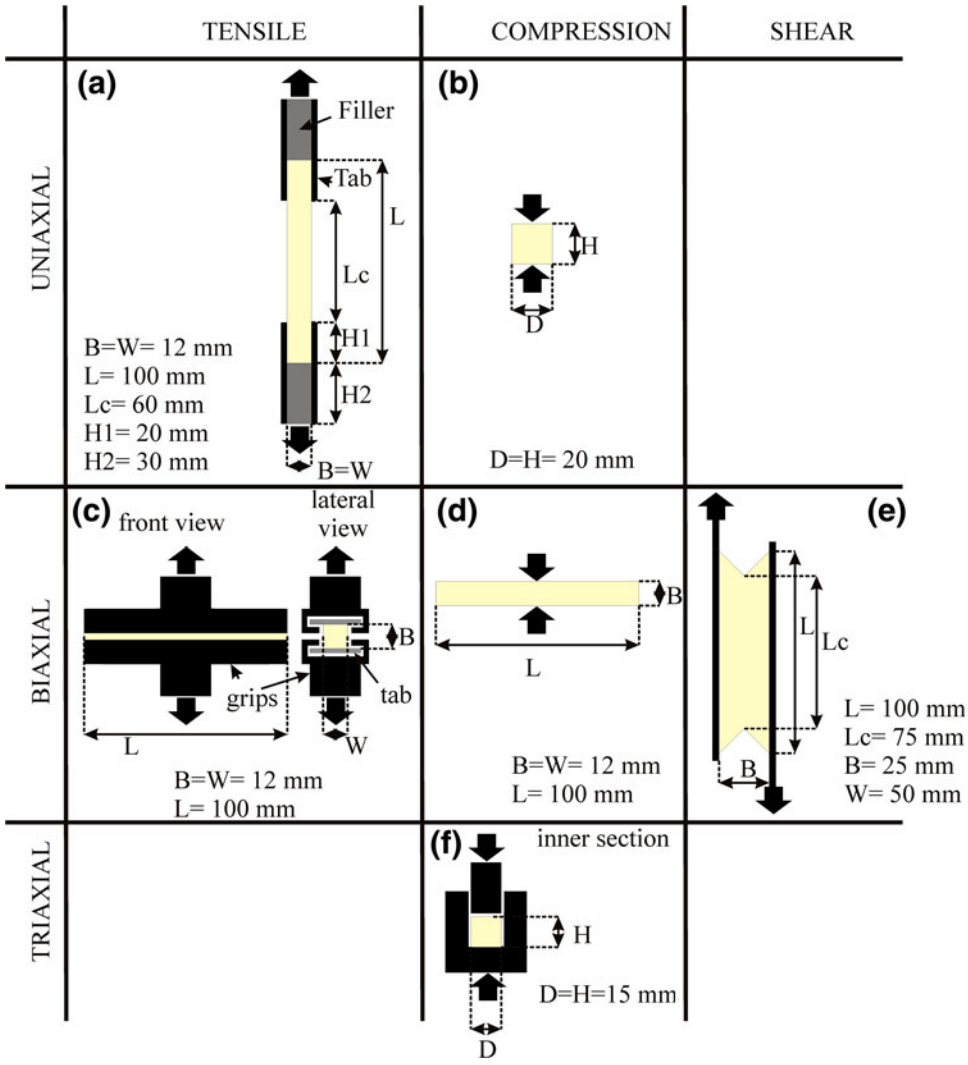

Fig. 2 Mechanical tests and specimens configuration

Uniaxial compression specimens were cylinders according to ISO 844:2004(E) (Fig. 2b).

The stresses developed during tests are depicted in Table 1.

2.2.2 Biaxial Tests. Prismatic strips were used for *restricted tension and compression* biaxial tests. Samples used for tensile tests were bonded to long glass/epoxy tabs. The specimens were subjected to uniaxial tensile (using on purpose made grips) or compressive stress along their length (Fig. 2c, d, respectively). As the specimens were loaded along its length, which is much larger than the other dimensions, it can be assumed that the strain along the longer dimension is zero and normal stress σ_2 deduced (see Table 1). The relationship between σ_2 and σ_1 given by Table 1 is only valid in the linear range of the stress-strain curve. The state of stress is uniform throughout most of the specimen away from the free edges, and the effect of the free edges can be considered negligible in view of the specimen dimensions.

Simple shear tests were performed according to ISO 1922:2001(E) (Fig. 2e). To avoid misalignments specimens were bonded to aluminum tabs. Shear stress is depicted in Table 1, while shear deformation γ was assessed from the array of points as the relative displacement of points in the applied load direction (1) divided by the width of the array of points in the TD (2), as

$$\gamma = \frac{\Delta\lambda_1}{\lambda_2} \qquad \text{(Eq 2)}$$

The rotation of the principal axes of the strain ellipsoid in simple shear (principal directions of the Euler finite strain tensor) during a plane shear test (Ref 27-30) must be taken into account. The angle α between the major (tensile) principal axis and the shear axis is calculated as:

$$\alpha = \frac{1}{2}\tan^{-1}\left(2/\gamma\right) \qquad \text{(Eq 3)}$$

The value of α decreased with γ, starting from $\alpha = 45°$. Simple shear curves were nearly linear up to brittle failure. All samples failed at 45° with respect to loading direction due to the tensile component of stress. For the low γ achieved, the angle between tensile principal axis and the shear axis at failure was $\alpha = 44.94°$. Therefore, rotation of principal axis was neglected.

Table 1 Principal stresses developed in different tests

	Tensile	Compression	Shear
Uniaxial	$\sigma_1 = FA_0(1+\varepsilon_2)(1+\varepsilon_3)$ $\sigma_2 = \sigma_3 = 0$	$\sigma_1 = FA_0(1+\varepsilon_2)(1+\varepsilon_3)$ $\sigma_2 = \sigma_3 = 0$	
Biaxial	$\sigma_1 = FA_0(1+\varepsilon_3)$ $\sigma_2 = \nu\sigma_1$ $\sigma_3 = 0$	$\sigma_1 = FA_0(1+\varepsilon_3)$ $\sigma_2 = \nu\sigma_1$ $\sigma_3 = 0$	$\tau = FWL_c$ $\sigma_1 = \tau$ $\sigma_2 = -\tau$ $\sigma_3 = 0$
Triaxial		$\sigma_1 = FA_0$ $\sigma_2 = \sigma_3 = \nu 1 - \nu\sigma_1$	

σ_1, σ_2, σ_3: true stresses in axial (1) and transverse (2 and 3) directions. τ: shear stress. F: current load applied to the specimen. A_0: initial cross section of the specimen. ε_2, ε_3: transverse strains. ν: Poisson's ratio. W, L_c: thickness and length of the calibrated part of shear specimen

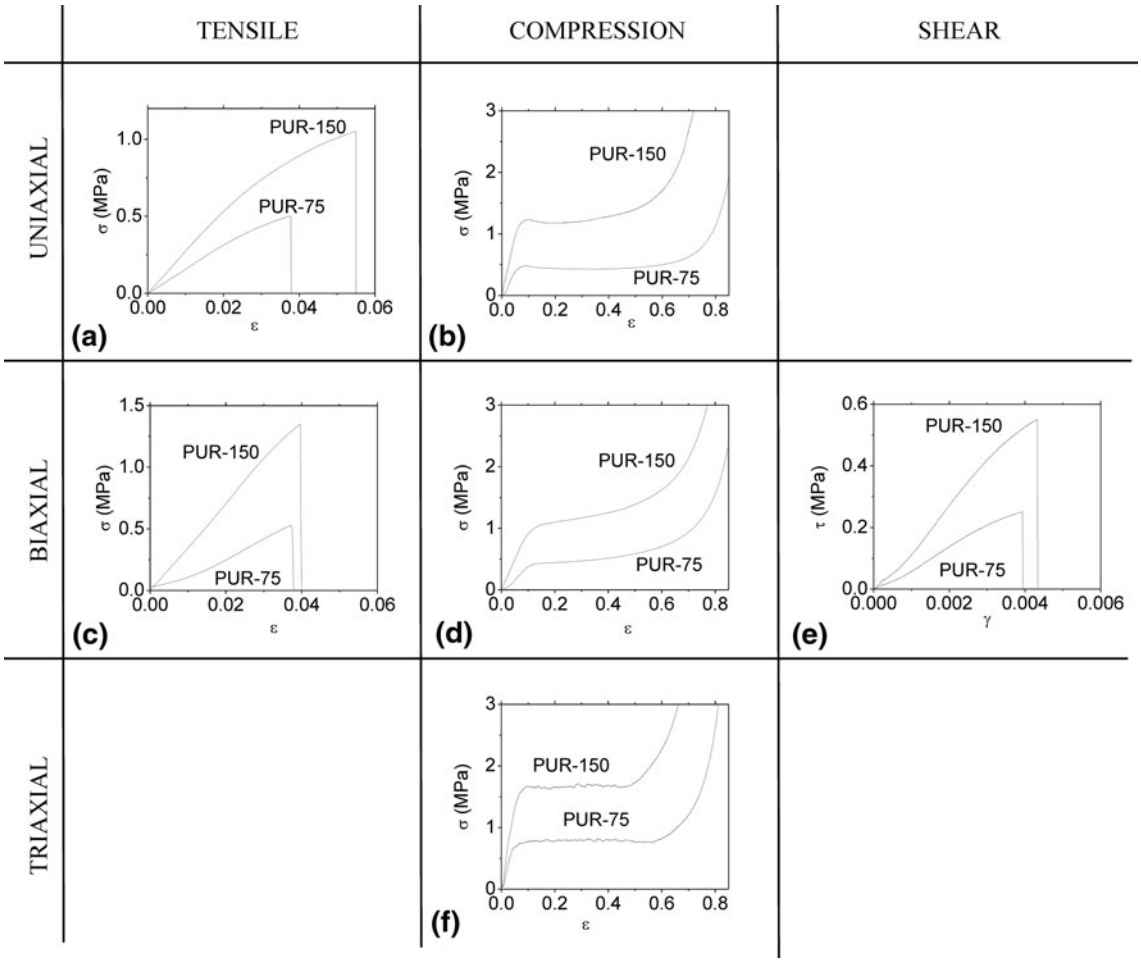

Fig. 3 Typical stress-strain curves obtained for PUR foams in GD at 1 mm/min: (a) uniaxial tension, (b) uniaxial compression, (c) restricted tension, (d) restricted compression, (e) simple shear, (f) confined compression

2.2.3 Triaxial Tests. *Confined compression* tests were performed using a cylindrical specimen and a specially constructed device (Fig. 2f). It consists of two steel plates with a cylinder-piston set attached to the bottom plate. The inner diameter of the cylinder is 15 mm with tolerances of −0.000 and +0.001 mm. The piston, to which compressive load was applied, was cut with a diameter of 15 mm with tolerances of +0.000 and −0.001 mm. The tight tolerances were necessary because of the extreme importance of providing no room for the foam to extrude during the test. The piston slid freely trough the hole when the bottom plate was removed, i.e., it is a frictionless device, but with the bottom plate attached, entrapped air retarded its movement, showing that the device and sample diameters were identical. Under such conditions, deformation in both TDs was prevented, i.e., $\varepsilon_2 = 0$ and $\varepsilon_3 = 0$. Replacing in elementary isotropic form of Hooke's law, i.e., $\varepsilon_1 = 1E(\sigma_1 - \nu(\sigma_2 + \sigma_3))$, $\varepsilon_2 = 1E(\sigma_2 - \nu(\sigma_1 + \sigma_3))$ and $\varepsilon_3 = 1E(\sigma_3 - \nu(\sigma_1 + \sigma_2))$, transversal stresses are obtained (Table 1). This relationship is strictly valid in the linear elastic range of stress-strain curve.

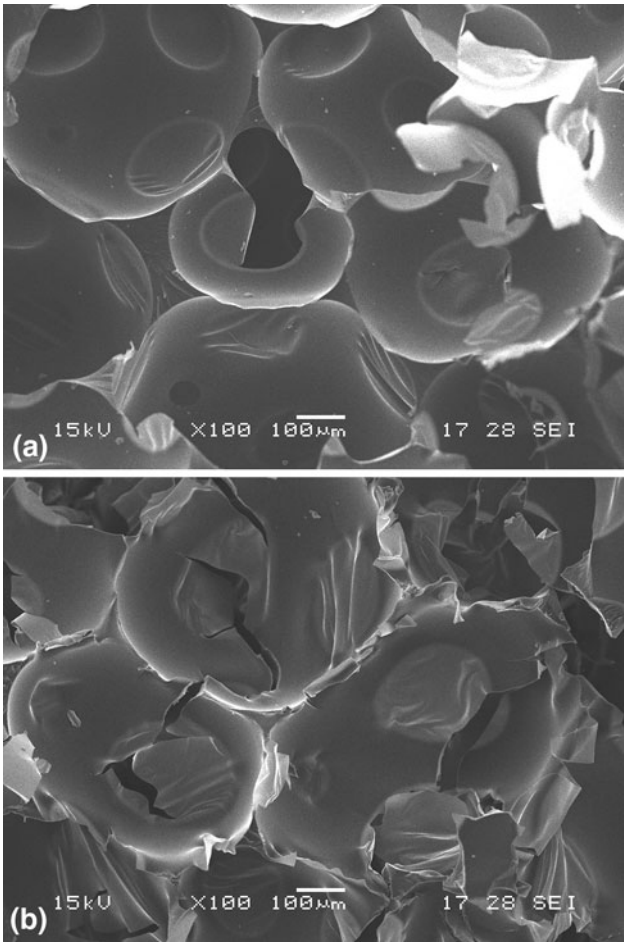

Fig. 4 SEM micrographs showing deformation features of broken samples under: (a) uniaxial tension and (b) uniaxial compression

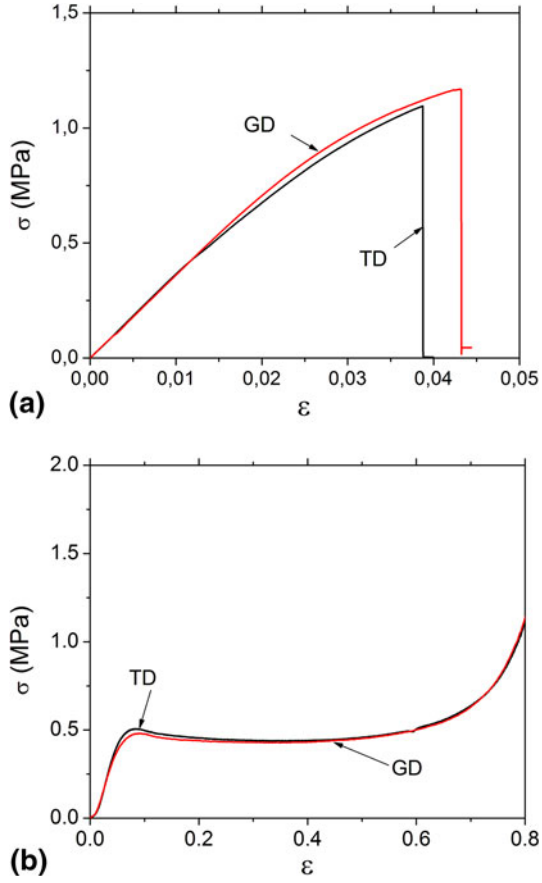

Fig. 5 Typical stress-strain curves obtained for PUR foams tested in different loading directions (GD and TD): (a) PUR-150 tested under uniaxial tension at 1 mm/min; (b) PUR-75 tested under uniaxial compression at 5 mm/min (Color figure online)

3. Results and Discussion

3.1 Phenomenology

Representative stress-strain curves are shown in Fig. 3 for PUR-75 and PUR-150 (GD, 1 mm/min). Both foams display analogous mechanical response. Uniaxial tensile, biaxial tensile (Fig. 3a, b), and simple shear (Fig. 3e) curves show a continuous increase in stress up to fracture. The stress-strain curves are almost all linear according to a cell wall bending mechanism. At a certain deformation level they become non-linear consistently with plastic cell face stretching. Curves terminate abruptly due to brittle fracture, which is attributable to propagation of pre-existing microcracks (Ref 31). Conversely, uniaxial, biaxial, and triaxial compression stress-strain curves show typical features of elasto-plastic behavior. The elastic linear part is followed by a non-linear one associated with plastic buckling of the cell walls. Then, the stress remains nearly constant due to plastic deformation accompanied with brittle crushing of the cells (Ref 31). Small oscillations in the plateau stress due to progressive crushing of the cells are particularly evident under the triaxial stress state (Fig. 3f). Finally, curves show a sharp raise caused by foam densification produced by collapse of cell structure and so that, the measured response corresponds to that of the cell material (Ref 22).

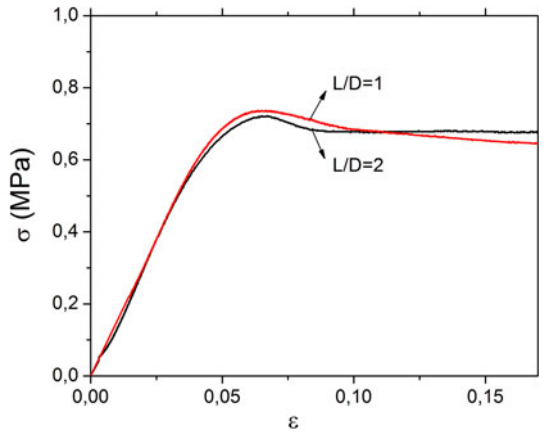

Fig. 6 Typical stress-strain curves obtained for PUR-75 under uniaxial compression using samples of different size (Color figure online)

Fracture surface features shown in Fig. 4 provide evidences of cell face stretching under tensile deformation (Fig. 4a) while plastic deformation and cell brittle crushing are detectable under compression (Fig. 4b). These observations confirm that the deformation mechanisms displayed by PUR foams are in agreement with those described in literature for other rigid polymeric foams.

Table 2 Failure stress values obtained under different test configurations for PUR foams tested at 1 mm/min

Test configuration	$\|\sigma_f\|$, MPa	
	PUR-75	PUR-150
Uniaxial tension	0.43 ± 0.01	0.94 ± 0.22
Uniaxial compression	0.62 ± 0.16	1.16 ± 0.16
Restricted tension	0.61 ± 0.11	1.22 ± 0.09
Restricted compression	0.47 ± 0.12	0.94 ± 0.07
Simple shear	0.31 ± 0.06	0.63 ± 0.07
Confined compression	0.62 ± 0.03	1.42 ± 0.08

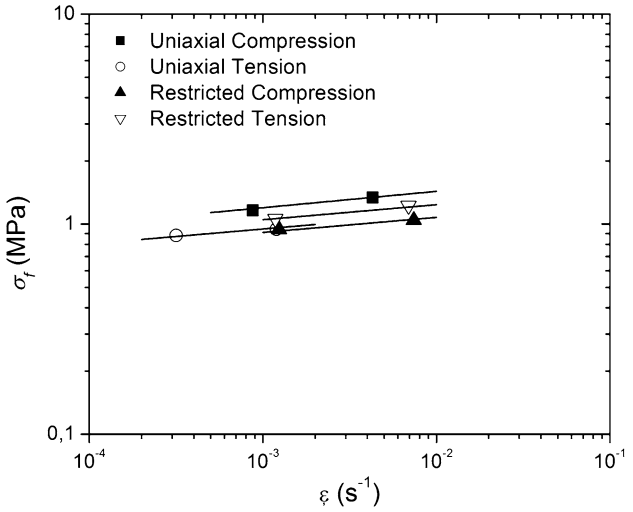

Fig. 7 Failure stress as a function of actual deformation rate for PUR-150

Increasing foam density enhances the initial stress-strain slope and the linear limit deformation as well as it lowers the strain at which densification starts in the compressive stress states.

As exemplified in Fig. 5, stress-strain curves obtained in TD are equivalent to those determined in GD indicating that the studied PUR foams are isotropic materials.

It is known that specimen size and volume are critical parameters for foam testing (Ref 17, 32-36). Individual cell in the foam has its own characteristic behavior under load. To assess foam bulk behavior enough cells have to deform together consistent with a continuum representation. As shown in Fig. 6, the uniaxial compression responses of samples having different aspect ratios are practically identical. About 40 cell diameters are included in the characteristic dimension of the smallest tested sample. This result indicates that the assessed mechanical behavior is independent of sample shape, volume and contour in all the used configurations.

3.2 Failure Criteria

In order to assess a failure criterion, it is first necessary to define the failure stress, σ_f. In the most general sense, failure is considered as the breakdown of linear elasticity (Ref 31) prior to the beginning of the plastic collapse of the foam. So that, in this work it is assumed that the failure stress coincides with the deviation from linearity of the measured stress-strain curves.

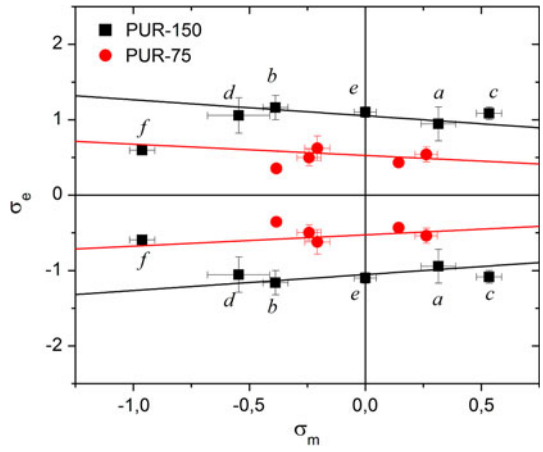

Fig. 8 Failure stress values under different stress states for PUR-75 and PUR-150 and Brittle Crushing failure envelopes (Eq 5). Failure points arise from: (a) uniaxial tension, (b) uniaxial compression, (c) restricted tension, (d) restricted compression, (e) simple shear, (f) confined compression

The failure stress values given in Table 2 were evaluated by the tangent method as previously done in literature for rigid foams (Ref 17, 23). In this method, the failure point (ε_f, σ_f) is determined from the intersection of two straight lines: one coincides with the linear elastic part and the other is a tangent to the curve drawn in the yield plateau or from the ultimate point depending on the stress-strain curve shape.

Due to the time-dependent behavior of polymers, it is important to evaluate the effect of deformation rate on failure data. As it is difficult to achieve the same deformation rate in all testing configurations, two crosshead speeds were used (1 and 5 mm/min) aiming to explore the dependency of failure stress over two decades of strain rate. The values of failure stress are plotted against the strain rate ($\dot{\varepsilon}$) in Fig. 7. It is verified that data follows a power law relationship:

$$\sigma_f = \sigma_0 \dot{\varepsilon}^m \qquad \text{(Eq 4)}$$

being σ_0 a reference stress, and m a strain rate sensitivity parameter. For all test configurations the m exponent is about 0.07. Therefore, it can be assumed that the influence of strain rate on failure stress is negligible within the testing range.

In light of the observed mechanical response of PUR foams (Fig. 3, 4), a criterion used to describe brittle crushing failure of metallic, ceramic, and polymeric foams (Ref 17, 23, 24, 31) was selected. This criterion assumes that under uniaxial loading the foam deforms primarily by bending of the cell walls, and under equal biaxial loading the bending stresses are suppressed and the cell walls stretch or compress uniaxially. The failure surface can be described as a function of the equivalent stress (σ_e) and the mean stress (σ_m) as:

$$\pm\frac{\sigma_e}{\sigma_{cr}^*} + 0.6\left(\frac{\rho}{\rho_s}\right)^{1/2}\frac{\sigma_m}{\sigma_{cr}^*} = 1 \qquad \text{(Eq 5)}$$

where

$$\sigma_e = \sqrt{\frac{(\sigma_1-\sigma_2)^2+(\sigma_2-\sigma_3)^2+(\sigma_1-\sigma_3)^2}{2}} \qquad \text{(Eq 6)}$$

and

$$\sigma_m = \frac{\sigma_1 + \sigma_2 + \sigma_3}{3} \quad \text{(Eq 7)}$$

The uniaxial collapse strength (σ^*_{cr}) is evaluated as the average of the failure stress determined under uniaxial compression (σ_{fc}) and uniaxial tension (σ_{ft}).

$$\sigma^*_{cr} = \frac{(\sigma_{ft} + \sigma_{fc})}{2} \quad \text{(Eq 8)}$$

Table 3 Stress points used to construct the Elastic Buckling criterion (Ref 5)

Stress state	σ_f/σ^*_{cr}
$\sigma_1 = \sigma_f$, $\sigma_2 = \sigma_3 = 0$	1
$\sigma_1 = \sigma_2 = \sigma_f$, $\sigma_3 = 0$	0.88
$\sigma_1 = \sigma_2 = \sigma_3 = \sigma_f$	0.83
$\sigma_1 = \sigma$, $\sigma_2 = \sigma_3 = -\sigma_f/8$	1.02
$\sigma_1 = -\sigma_f/2$, $\sigma_2 = \sigma_3 = \sigma_f$	0.90

The value of σ^*_{cr} is the uniaxial collapse strength given by Eq 8

The ratio ρ/ρ_s is the relative density of the foam, in particular for a rigid polyurethane the polymer density is ρ_s = 1200 kg/m^3 (Ref 37).

The failure envelopes arisen from the brittle crushing criteria of PUR-75 and PUR-150 foams are drawn in the $\sigma_e - \sigma_m$ space in Fig. 8. This criterion is able to describe failure data for restricted tension and simple shear but fails to do so for restricted and confined compression. This fact can be attributed to different failure mechanisms acting under constrained compressive stress states. Under such loading conditions, foam deformation may be governed by elastic buckling of the cell walls instead of by cell wall bending.

To take into account this possible change in deformation mechanisms, a criterion for elastic buckling (buckling cap) proposed by Gibson et al. (Ref 9) is chosen. The failure cap has not a simple mathematical expression but it can be easily constructed from particular stress states points, previously calculated by Triantafillou et al. (Ref 5). The construction points are listed in Table 3.

Elastic buckling caps of PUR-75 and PUR-150 are plotted together with the brittle crushing envelopes in Fig. 9. The Buckling cap is capable to describe quite well the compression failure data that are not captured by the brittle crushing failure

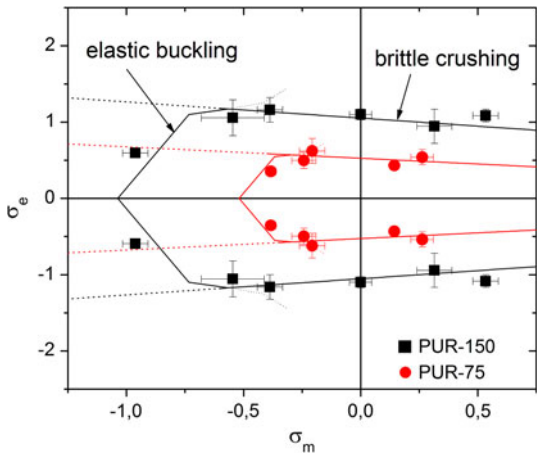

Fig. 9 Multiaxial failure of PUR-75 and PUR-150 described by Brittle Crushing and Elastic Buckling criteria

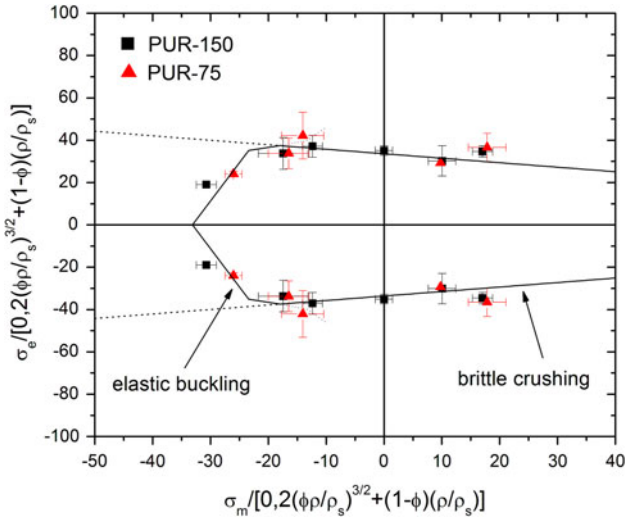

Fig. 11 Generalized multiaxial failure criterion for PUR foams

Stress state	σ_{fs} (MPa)
a) Uniaxial tension	30.01
b) Uniaxial compression	-37.99
c) Restricted tension	39.43
d) Restricted compression	-30.50
e) Simple shear	20.26
f) Confined compression	-44.72

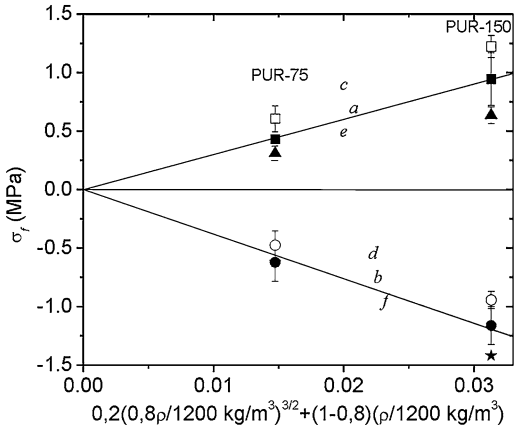

Fig. 10 Failure stress data plotted as a function of foam relative density according to Eq 9. Letters indicate the stress state: (a) uniaxial tension, (b) uniaxial compression, (c) restricted tension, (d) restricted compression, (e) simple shear, (f) confined compression

criterion. In summary, to assess the multiaxial failure of PUR foams it is necessary to combine both brittle crushing and elastic buckling criteria. This result indicates that under constrained compressive stress states the source of non-linearity is related to elastic buckling of the cells.

Failure envelopes of PUR-75 and PUR-150 appeared to be self similar (Fig. 9). As well, increasing density does not change the mechanical response of PUR foams (Fig. 3). So, in order to obtain a general failure surface for rigid PUR foams, the dependency of foam failure stress on its relative density must be included.

For foams exhibiting brittle crushing a relationship between failure stress, σ_f, and relative density, ρ/ρ_s has been proposed (Ref 31):

$$\sigma_f = \sigma_{fs}\left[0.2\left(\phi\frac{\rho}{\rho_s}\right)^{3/2} + (1-\phi)\left(\frac{\rho}{\rho_s}\right)\right] \quad \text{(Eq 9)}$$

where σ_{fs} is the modulus of rupture of the cell wall material for each stress state. This theoretical model considers the foam as a cubic array of members of length l and square cross section of side t in which adjoining cells are staggered so that their members meet at their midpoints. In the case of closed-cell foams a fraction ϕ of the solid is contained in the cell edges and the remaining fraction $(1-\phi)$ is in the cell faces. The fraction ϕ is typically 0.8 for rigid polyurethane foams with relative density below 0.4 (Ref 38). Failure stress data are plotted according to Eq 9 in Fig. 10. This model well describes the effect of foam density on failure stress data for all stress states. The values of σ_{fs}, determined by linear regression, are included in Fig. 10.

According to the observed behavior (Fig. 10), all stress values can be normalized by Eq 9 as follows:

$$\sigma_i^N = \frac{\sigma_i}{0.2\left(\phi\frac{\rho}{\rho_s}\right)^{3/2} + (1-\phi)\left(\frac{\rho}{\rho_s}\right)} \quad \text{(Eq 10)}$$

Using normalized stresses, a generalized failure criterion is easily obtained, as shown in Fig. 11. This failure criterion results from the combination of brittle crushing and elastic buckling models and takes into account the foam relative density. Further, the low strain rate sensitivity displayed by PUR foams in the studied range suggests that they can be approximated as rate independent materials. So, the obtained generalized failure criterion is adequate to establish PUR foams failure limits in most practical applications. The applicability this approach is defined by the linearity of deformation micromechanisms. If non-linear micromechanisms develop at early stages of foam deformation, compromising the whole stress-strain behavior, the approach would be no longer valid. Regarding cell wall thickness or size, the approach will be valid as long as the assumptions made in the model development (Ref 31) are met.

4. Summary and Conclusions

Through this work the multiaxial deformation behavior of two commercial rigid polyurethane foams was determined. The data arose from simple experimental tests performed in a standard uniaxial universal testing machine. The specimen configurations used allowed generating suitable data under uniaxial, biaxial, and triaxial stress states. These stress states could be reached by using suitable testing fixtures which implied the use of special grips and lateral restricted samples. Actual strains were monitored with a video extensometer.

It was shown that the foams exhibited typical isotropic brittle behavior, except under compressive loading in which the response turned out to be ductile. Failure was governed by cell wall bending, cell face stretching, and brittle fracture under tensile loading, while cell wall bending and buckling followed by brittle crushing were dominant under compressive loads.

The failure stress defined as the limit of stress-strain linear proportionality depended on the relative density of foams according to a model for brittle crushing proposed by Gibson and Ashby. The combination of a simple theoretical criterion developed in literature for brittle crushing of closed-cell cellular materials capped by an elastic buckling criterion was able to well describe all the experimental failure data of PUR foams.

Based on the mentioned criteria a general failure envelope to predict the safety limits of PUR foams of relative low density under multiaxial loading conditions was successfully constructed from the generated data.

Acknowledgments

Authors would like to thank CONICET and ANPCyT from Argentina for financial support.

References

1. J. Zhang and M.F. Ashby, Mechanical Selection of Foams and Honeycombs Used for Packaging and Energy Absorption, *J. Mater. Sci.*, 1994, **29**(1), p 157–163
2. M. Avalle, G. Belingardi, and R. Montanini, Characterization of Polymeric Structural Foams Under Compressive Impact Loading by Means of Energy-Absorption Diagram, *Int. J. Impact Eng.*, 2001, **25**(5), p 455–472
3. H. Zhao, G. Gary, and J.R. Klepaczko, On the Use of a Viscoelastic Split Hopkinson Pressure Bar, *Int. J. Impact Eng.*, 1997, **19**(4), p 319–330
4. *Polyurethane Handbook*, 2nd ed., G. Oertel, Ed., Hanser, Munich, 1993
5. T.C. Triantafillou, J. Zhang, T.L. Shercliff, L.J. Gibson, and M.F. Ashby, Failure Surfaces for Cellular Materials Under Multiaxial Loads-II. Comparison of Models with Experiment, *Int. J. Mech. Sci.*, 1989, **31**, p 665–678
6. G. Menges and F. Knipschild, Estimation of Mechanical Properties for Rigid Polyurethane Foams, *Polym. Eng. Sci.*, 1975, **15**(8), p 623–627
7. A.T. Huber and L.J. Gibson, Anisotropy of Foams, *J. Mater. Sci.*, 1988, **23**(8), p 3031–3040
8. F. Saint-Michel, L. Chazeau, J.-Y. Cavaillé, and E. Chabert, Mechanical Properties of High Density Polyurethane Foams: I. Effect of the Density, *Compos. Sci. Technol.*, 2006, **66**(15), p 2700–2708
9. L.J. Gibson, M.F. Ahsby, J. Zhang, and T.C. Triantafillou, Failure Surfaces for Cellular Materials Under Multiaxial Loads-I. Modelling, *Int. J. Mech. Sci.*, 1989, **31**(9), p 635–663
10. M. Zaslawsky, Multiaxial-Stress Studies on Rigid Polyurethane Foam, *Exp. Mech.*, 1973, **13**(2), p 70–76
11. P.S. Theocaris, The Influence of Porosity on the Failure Behaviour of Foams, *Int. J. Damage Mech.*, 1998, **7**(4), p 301–331
12. D.-A. Wang and J. Pan, A Non-Quadratic Yield Function for Polymeric Foams, *Int. J. Plast.*, 2006, **22**(3), p 434–458
13. Y. Kim and S. Kang, Development of Experimental Method To Characterize Pressure-Dependent Yield Criteria for Polymeric Foams, *Polym. Test.*, 2003, **22**(2), p 197–202
14. R.E. Miller, A Continuum Plasticity Model for the Constitutive and Indentation Behaviour of Foamed Metals, *Int. J. Mech. Sci.*, 2000, **42**(4), p 729–754
15. V.S. Deshpande and N.A. Fleck, Isotropic Constitutive Models for Metallic Foams, *J. Mech. Phys. Solids*, 2000, **48**(6–7), p 1253–1283

16. L.W. Hu and K.D. Pae, Inclusion of the Hydrostatic Stress Component in Formulation of the Yield Condition, *J. Frankl. Inst.*, 1963, **275**(6), p 491–502
17. D. Ruan, G. Lu, L.S. Ong, and B. Wang, Triaxial Compression of Aluminium Foams, *Compos. Sci. Technol.*, 2007, **67**(6), p 1218–1234
18. T.C. Triantafillou, J. Zhang, T.L. Shercliff, L.J. Gibson, and M.F. Ashby, Failure surface for Cellular Materials Under Multiaxial Loads II. Comparison of Models with Experiment, *Int. J. Mech. Sci.*, 1989, **31**(9), p 665–678
19. J. Zhang, N. Kikuchi, V. Li, A. Yee, and G. Nuscholtz, Constitutive Modeling of Polymeric Foam Material Subjected to Dynamic Crash Loading, *Int. J. Impact Eng.*, 1998, **21**(5), p 369–386
20. V.L. Tagarielli, V.S. Deshpande, N.A. Fleck, and C. Chen, A Constitutive Model for Transversely Isotropic Foams, and Its Application to the Indentation of Balsa Wood, *Int. J. Mech. Sci.*, 2005, **47**(4-5), p 666–686
21. D. Zenkert and M. Burman, Tension, Compression and Shear Fatigue of a Closed Cell Polymer Foam, *Compos. Sci. Technol.*, 2009, **69**(6), p 785–792
22. E.E. Gdoutos, I.M. Daniel, and K.A. Wang, Failure of Cellular Foams Under Multiaxial Loading, *Compos. A Appl. Sci. Manuf.*, 2002, **33**(2), p 163–176
23. G. Gioux, T.M. McCormack, and L.J. Gibson, Failure of Aluminum Foams Under Multiaxial Loads, *Int. J. Mech. Sci.*, 2000, **42**(6), p 1097–1117
24. V.S. Deshpande and N.A. Fleck, Multi-Axial Yield Behaviour of Polymer Foams, *Acta Mater.*, 2001, **49**(10), p 1859–1866
25. H. Jin, W.-Y. Lu, S. Scheffel, T. Hinnerichs, and M. Neilsen, Full-Field Characterization of Mechanical Behaviour of Polyurethane Foams, *Int. J. Solids Struct.*, 2007, **44**(21), p 6930–6944
26. W. Gemin, V. Pettarin, L. Fasce, A. Tami, P. Frontini, *Medición del comportamiento mecánico de materiales con técnicas de video (Assessment of Materials' Mechanical Behavior with Video Techniques)*, R. Romero, A. Cuniberti Eds., PropMec'05, UNCPBA Ed., 2006, p 91–96 (in Spanish)
27. C. G'Sell, S. Boni, and S. Shrivastava, Equivalent Strain in Large Deformation Torsion Testing: Theoretical and Practical Considerations, *J. Mech. Phys. Solids*, 1982, **30**(1-2), p 75–90
28. G.R. Canova, S. Shrivastava, J.J. Jonas, C. G'Sell, The Use of Torsion Testing to Assess Material Formability, *Formability of Metallic Materials—2000 A.D.*, J.R. Newby, B.A. Niemer, Ed., American Society for Testing and Materials, Metals Park, Ohio, 1982, p 189
29. J.C. Jaeger, *Elasticity, Fracture and Flow*, Chapman and Hall, London, 1969
30. C. G'Sell and A.J. Gopez, Plastic Banding in Glassy Polycarbonate Under Plane Simple Shear, *J. Mater. Sci.*, 1985, **20**(10), p 3462–3478
31. L.J. Gibson and M.F. Ashby, *Cellular Solids. Structure and Properties*, Cambridge University Press, London, 1999
32. J.F. Rakow and A.M. Waas, Size Effects and the Shear Response of Aluminum Foam, *Mech. Mater.*, 2005, **37**(1), p 69–82
33. J.F. Rakow and A.M. Waas, Size Effects in Metal Foam Cores for Sandwich Structures, *Am. Inst. Aeronaut. Astronaut. J.*, 2004, **42**(7), p 1331–1337
34. Z.P. Bažant, Y. Zhou, G. Zi, and I.M. Daniel, Size Effect and Asymptotic Matching Analysis of Fracture of Closed-Cell Polymeric Foam, *Int. J. Solids Struct.*, 2003, **40**(25), p 7197–7217
35. Z.P. Bažant, Y. Zhou, D. Novák, and I.M. Daniel, Size Effect in Fracture of Sandwich Structure Components: Foam and Laminate, *Am. Soc. Mech. Eng. Appl. Mech. Div.*, 2001, **248**, p 19–30
36. E.W. Andrews, G. Gioux, P. Onck, and L.J. Gibson, Size Efects in Ductile Cellular Solids. Part II: Experimental Results, *Int. J. Mech. Sci.*, 2001, **43**, p 701–713
37. P.J. Phillips and N.R. Waterman, The Mechanical Properties of High-Density Rigid Polyurethane Foams in Compression: I. Modulus, *Polym. Eng. Sci.*, 1974, **4**(1), p 67–71
38. D.W. Reitz, M.A. Schnetz, and L.R. Glicksman, A Basic Study of Aging of Foam Insulation, *J. Cell. Plast.*, 1984, **20**(2), p 104–113